CHARGE DISTRIBUTION IN $^{40}Ar + {}^{159}Tb$ REACTION AT 9.5 MeV/NUCLEON

E. KOZIK[a], J. BŁOCKI[b], A. BUDZANOWSKI[a], J. GALIN[c],

D. HILSCHER[d], H. HOMEYER[d], U. JAHNKE[d], T. KOZIK[e], Z. SOSIN[e]

[a] H. Niewodniczański Institute of Nuclear Physics
Radzikowskiego 152, 31-342 Cracow, Poland
[b] Institute for Nuclear Studies, 05-400 Świerk, Poland
[c] GANIL, Caen Cedex, France
[d] Hahn-Meitner Institut, Berlin, Germany
[e] Institute of Physics, Jagellonian University
Reymonta 4, 30-059 Cracow, Poland

(Received July 1, 1996)

Two models were applied to reproduce the experimentally obtained charge distribution for $^{40}Ar+{}^{159}Tb$ system at 9.5 MeV/nucleon. They are based on either random walk phenomena or on one body dissipative processes. The charge numbers of measured outgoing fragments were in the range of $Z = 7 - 20$. The model taking into account the differences in the density of final states of the heavier and lighter ions appeared to be suitable for the description of peripheral collisions. The drift of the mass and charge is expected towards asymmetric division, producing in the exit channel the projectile-like fragments lighter than the projectile. In order to compare the model calculations with experimental data the statistical deexcitation of the primary hot fragments has been taken into account. The succesfull description of the data by the proposed model supplemented by statistical evaporation ilustrates the great importance of the phase space factors for directing the mass and charge flow in pheripheral and damped heavy ion collisions.

PACS numbers: 25.70.Hi,25.70.Lm

1. Introduction

Reactions between two heavy ions at energies of a few MeV/nucleon above the Coulomb barrier lead mainly to the binary processes [1]. In the exit channel projectile-like and target-like fragments (PLF and TLF) occur

with the final energy ranging from that of the entrance channel down to the Coulomb barrier energy and even below. These phenomena are somewhat arbitrary classified as quasi elastic (QE), deep inelastic (DIC) or strongly damped collisions. Although a considerable overlap of the nuclear matter densities of the projectile and the target takes place with decreasing impact parameters the participating ions do not loose completely their identities. At small impact parameters the compound nucleus formation instead of the formation of short-lived dinuclear system is observed. The reaction scenarios which clearly distinguish binary processes and the complete fusion become invalid at higher energies. At projectile velocity approaching the velocity of sound in nuclear matter (corresponding to an energy around 14 MeV/nucleon) new processes appear. These are nonequilibrium emission of nucleons or clusters, projectile break-up and multifragmentation of the entire system considered as a sort of liquid to gas phase transition of highly excited nuclear matter [2–4].

In recent years a number of models have been developed to explain the mechanism of peripheral and damped heavy ion reactions. These models may be divided into two basic categories. The first category of models is based on the assumption that the reaction mechanism is governed by a mean field effects. The individual nucleon-nucleon interaction is suppresed by the Pauli principle and the dissipative processes are described by the "one body" formalism [5–7]. The second category of models assumes that in heavy ion collisions the energy dissipation proceeds vastly by stochastic transfer of nucleons caused by individual nucleon-nucleon interaction. These models are especially suitable for description of peripheral collisions at sufficiently high energies, where the Pauli blocking becomes less effective [8–10].

In the present paper the performance of the two models belonging to both categories described above is verified experimentally. The studied ^{40}Ar + ^{159}Tb reaction at 9.5 MeV/nucleon shows the preponderance of the binary exit channels matching then the postulates of the verified models.

In Sec. 2 we present in some details the experimental procedure and the description of the apparatus. The brief overwiev of the experimental results which includes the charged particle spectra and neutron multiplicities as a function of the detected PLF's kinetic energy is presented in Sec. 3. Sec. 4 contains a concise characteristics of the applied models with special emphasis on some aspects which differ them. In Sec. 5 we present a discussion of the confrontation of the models with the experimental charge distribution of projectile-like fragments. Finally, the conclusions are summarized in Sec. 6.

2. Experimental setup

The experiment was performed at the Hahn-Meitner Intitute in Berlin using 380 MeV ^{40}Ar ions beam from the VICKSI heavy ion accelerator.

Neutrons released simultaneously from the $^{40}Ar + ^{159}Tb$ collision were detected in coincidence with the projectile-like fragments (PLF) emitted in laboratory frame at 14.5° with respect to the beam axis in horizontal plane. Projectile-like fragments were detected with conventional solid state silicon ΔE-E telescope detector which subtended the solid angle of 3 msr. The ΔE-E detectors had the thickness of 25 and 1000μ, respectively, what is sufficient to stop all the particles of interest. The fragments were identified by charges in the range of $Z_{PLF} = 7$–20 and the low energy threshold varied from 30 MeV for $Z_{PLF} = 7$ up to 150 MeV for $Z_{PLF} = 20$. The PLF detection signal from the telescope detector was used as a trigger for the registration of coincident neutrons. For the 4π neutrons detection the scintillator tank of 1 meter diameter filled with 500 l of toluen (C_7H_8) enriched by adding 0.5% (by weight) of ^{nat}Gd was used [11]. The trigger signal from the telescope detector started the 35μs-long counting period for the neutrons detection. The efficiency of neutrons detection was determined in the present experiment to be approximately 82%. The selfsupporting ^{159}Tb target used in the measurement was 524 $\mu g/cm^2$ thick. The beam was monitored by the additional telescope detector placed at the polar angle of 8° in laboratory frame.

The experimental data were recorded event-by-event on the data disc and the analysis and the reconstruction of events were performed off-line. A complete description of the experimental setup will be published elsewhere [12].

3. Experimental results

The energy loss in the ΔE transmission detector together with the energy deposit in the E stopping detector was converted event-by-event into kinetic energy and atomic number of the registered PLF. The accompanying neutron multiplicities were used for the reconstruction of the neutron fold.

The energy spectra of the PLF's recorded at $\theta_{lab} = 14.5° \pm 1.7°$ are shown in Fig. 1. The Coulomb barriers between PLF and the remnant of the system are marked by downward pointing arrows. The upward pointing arrows mark the energy corresponding to the beam velocity assuming the $A_{PLF} = 2Z_{PLF} + 1$. The smooth evolution of the shape of the energy spectra is seen as a function of the atomic number of PLF. The characteristic features of the spectra are as follows:

— for the exit channels where only few nucleons are removed from the projectile, two components of the energy spectra are clearly distinguished. The first one is concentrated at the energy below that corresponding to the beam velocity, the second one at energies near the exit channel Coulomb barrier. With decreasing PLF charge number the overlap

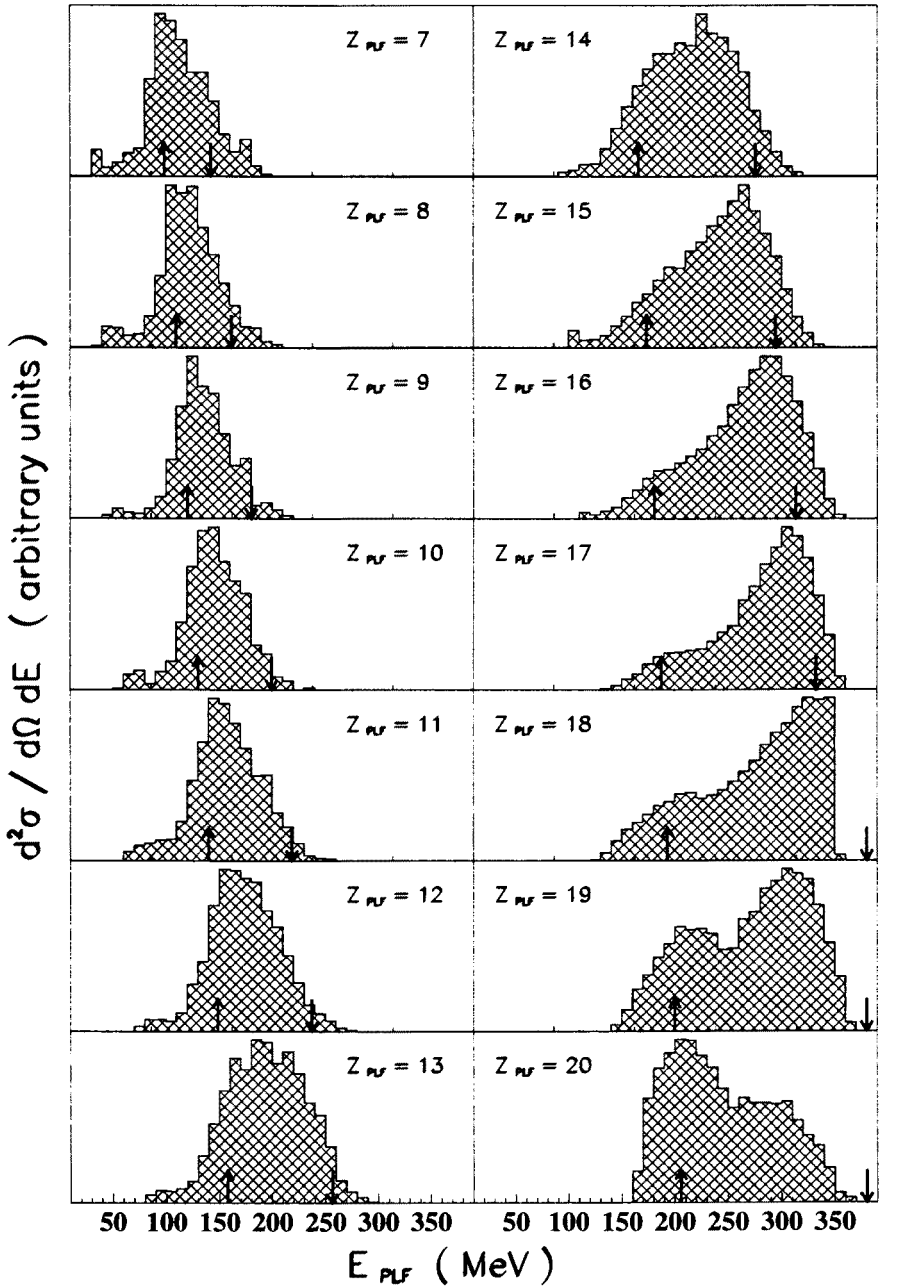

Fig. 1. Energy spectra of PLF's with Z values ranging from 7 to 20 integrated in 10 MeV bins of ejectile energy. The arrows indicate the Coulomb barrier and the energy corresponding to the beam velocity.

of both components becomes significant. For $Z_{\mathrm{PLF}} < Z_{\mathrm{proj}}$ close to the projectile charge number the intensity of low energy component is small in comparison to the high energy part. In the energy spectra of PLF's with $Z_{\mathrm{PLF}} = 19$ the intensities of high and low energy events are comparable, while for $Z_{\mathrm{PLF}} = 20$ the low energy component becomes predominant. For PLF's far from the projectile charge only one component in the energy spectra spreaded between the Coulomb barrier and beam energy is observed.

— the products with energies considerably below the Coulomb barrier as well as the products with energies above that correspondig to the beam velocity are also observed for all $Z_{\mathrm{PLF}} < Z_{\mathrm{proj}}$.

In Fig. 2. contour plots of neutron multiplicity versus kinetic energy of fragments are presented for selected $Z_{\mathrm{PLF}} = 7, 10, 13, 14, 17, 19$. The choice of presented contour plots corresponds to the various regions of Z_{PLF}. The maps for PLF charge close to the Z_{proj}, for atomic number from intermediate region of Z_{PLF} (for which the change of the energy spectra character is observed, see Fig. 1.) and for smallest PLF charge numbers are demonstrated, reflecting the neutron multiplicity dependence on PLF kinetic energy in the whole range of the measured Z_{PLF}. It can be concluded that the reaction mechanism leading to the production of different PLF's is composed. For lowest charges of PLF's three islands on the contour plot are well separated and labeled with letters A,B and C. The events of type A are characterized by the highest neutron multiplicity indicating on the strong energy damping — this process dominates quantitatively. The events of type B are grouped in the vicinity of the beam velocity and occur with small neutron multiplicity. The most likely origin of this events is therefore the projectile breakup. This nearly cold fragmentation of the projectile disapears from the experimental data with increasing Z_{PLF}. The events of type C are localized at lowest kinetic energies in the close vicinity of two body exit channel Coulomb barrier.This suggests the compound nucleus evaporation as a source of C-type events. The evaporation of massive intermediate mass fragments (IMF) exhausts the vast part of the compound nucleus excitation energy resulting then in a low neutron multiplicity. The low energy IMF's accompanied with a few registered neutrons may also origin from cold splitting of the projectile and the undetected second fast fragment takes off the missing energy.

The general character of the contour plots presented in Fig. 2. becomes succesively more unique with increasing Z_{PLF}. For PLF's close to the projectile charge the processes with small energy damping are overwhelming other exit channels except the case of $Z_{\mathrm{PLF}} = 20$, where the strongly damped events are predominant (see Fig. 1.). The mostly damped collisions consequently are accompanied by the highest neutron multiplicity.

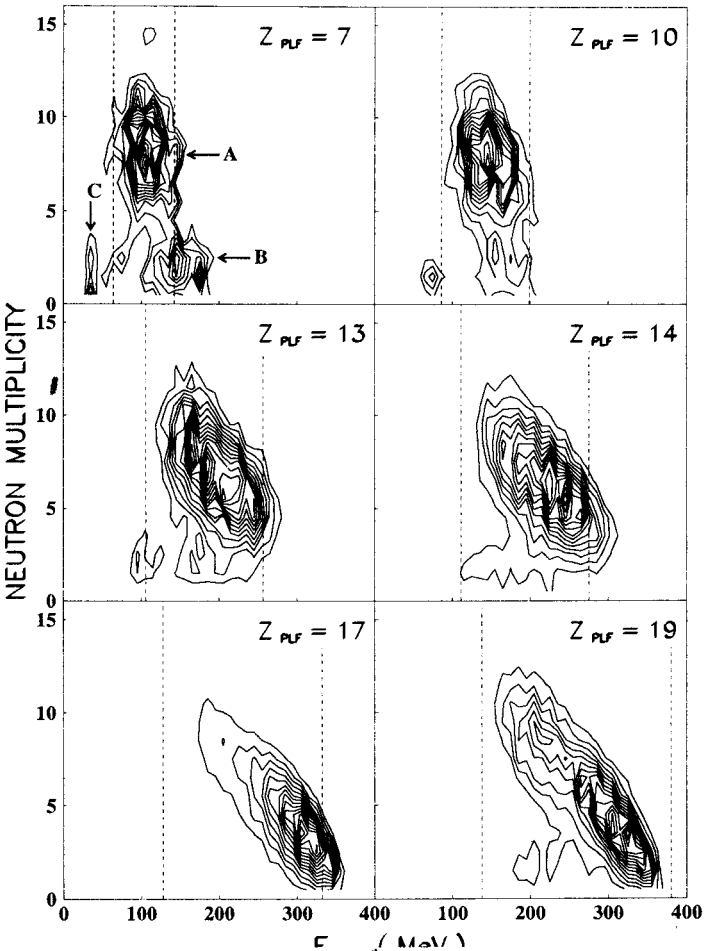

Fig. 2. Contour plots of counts as a function of measured PLF kinetic energy and neutron multiplicity for selected Z values. The meaning of A, B, C letters is described in the text. The dashed lines correspond to the arrows from Fig. 1

The characteristic feature of contour plots presented in Fig. 2. is the broad distribution of events in the energy space.

The corresponding experimental charge distribution is presented and discussed in Sec. 5.

4. Models

The model of deep inelastic collisions was applied to obtain cross sections for different PLF products observed experimentally (Z = 7-20). In the model the one-body dissipation mechanism was assumed in which in the first stage of the collision the main mechanism of energy dissipation is

the exchange of particles between two colliding ions [7]. In the later stage as the distribution of the momenta of particles (nucleons) is relaxed the wall formula [6] mechanism of dissipation is taking over. The model is strictly a classical one where Rayleigh–Lagrange equations of motion are solved for the properly parametrized nuclear shapes [13], which are axially symmetric. For the conservative forces a model of the folding potential [14] and for the moments of inertia the Werner–Wheeler mass flow approximation are applied. The system of the Rayleigh–Lagrange equations of motion is solved numerically from the point where two ions start to feel their mutual nuclear interaction up to the point where they reseparate again. Calculations have been done in the broad range of the incoming angular momentum L from $90\hbar$ to $205\hbar$. Below this range there is a fusion of two colliding ions and above this range the elastic scattering prevails. As the flow of particles is essentially the same in both directions (from target to projectile and opposite to it), due to the conservative forces, the drift predicted by such a model is towards mass symmetry. So one is unable to form ions much lighter than the projectile ($Z = 18$). In the region of high angular momenta L above $180\hbar$ the fragments close to the projectile are produced with the excitation energies up to 40 MeV. One could then expect after the evaporation the fragments in the most one or two units in Z lower than the projectile which is still far away from the low Z fragments observed in the experiment. Therefore one could say that the scope of the model is limited to that part of data which leads to the production of fragments heavier than the projectile. The only way to go towards more asymmetric splitting of ions is to include the statistical effects which would broaden the distribution of Z in both directions around the projectile. As can be seen from Fig. 3 the model works quite well in the region of $Z_{\mathrm{PLF}} \geq Z_{\mathrm{proj}}$ however the experimental limitations do not allow for more extended comparison. The results of the model calculations are denoted in Fig. 3. by the stars. One should also keep in mind that in the experiment the detecting system for PLF's is placed at $\theta_{\mathrm{lab}} = 14.5°$, whereas fragments produced in the model are spread over the whole region of angles (0°–180°).

Taking into account the foregoing arguments we attempted to describe the data with another approach which has an inherent feature of the mass drift from the projectile to the target. The model is described in Ref. [15] and here we shall specify only its important characteristics [16]. It assumes that nucleons in the course of the collision of two ions are transferred from target to projectile and vice versa in a way which reflects the size of the available phase space in both ions. As the phase space of the heavier ion (target) is larger then the phase space of the projectile the flow of the nucleons in the direction from the projectile to the target is more favoured than in the opposite direction. Similar idea was succesfully applied by

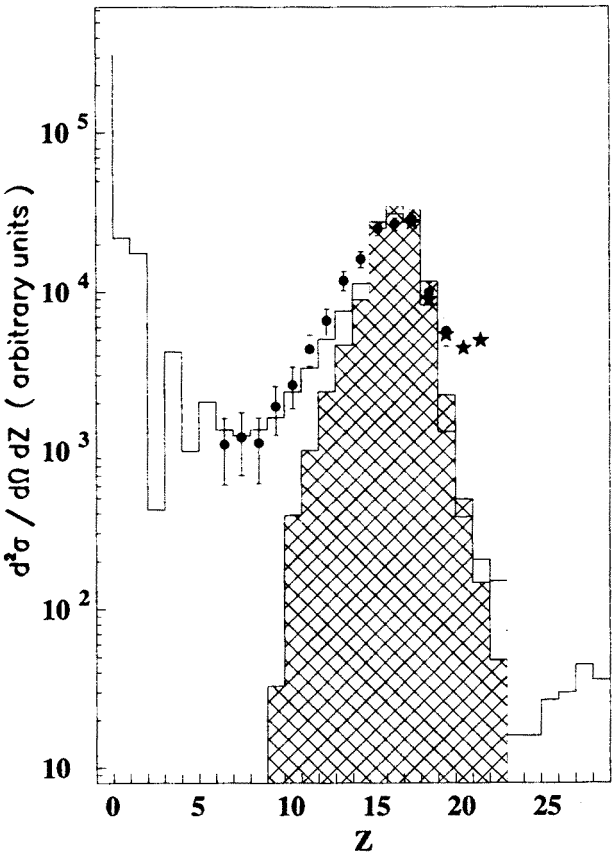

Fig. 3. Charge distributions for $^{40}Ar+^{159}Tb$ collision at 14.5°. The dots represent the experimental results. The hatched and empty histograms denote the pure model calculation and calculation including the statistical evaporation, respectively. The results obtained using the deep inelastic model are denoted by stars. The bars represent the statistical errors.

Wilczynski *et al.* [17] in the "sum rule model" of deep inelastic collisions. In this way we can expect that in the peripheral collisions for which the model is especially applicable the drift in mass and charge is towards more asymmetric division.

In the model it is assumed that the transfer of nucleons is a two-step process. In the first step when two potentials corresponding to the target and the projectile start to overlap certain amount of nucleons is perturbated and brought from the state in one of the potentials to a virtual state in the overlapping region. At this stage of the reaction these disturbed nucleons belong neither to the projectile nor to the target and they are bound by the mean field of the entire system. The disturbance and the transfer of nucleons

to the virtual region are caused by the mean field of both nuclei and by the two body nucleon-nucleon interactions. In the next step nucleons from this virtual state are transferred either to the PLF or TLF with a probability proportional to the density of states in both ions.

The proposed model is capable to calculate mass, charge, energy and angular distributions and to determine an excitation energy partition between projectile-like and target-like fragments in a consistent way.

5. Discussion

We have performed the Monte Carlo calculations of this two step process and the results are presented in Fig. 3. The Z - distribution shown as the hatched histogram is a pure result of the random walk model calculations. It reflects the binary division of the available mass and charge into excited primary PLF and TLF. As both PLF and TLF are excited and therefore evaporate particles, we have applied an evaporation code to simulate the deexcitation process along a sequential decay cascade [18]. The charge distribution of cold remnants obtained in that way is shown in Fig. 3 as the empty histogram. Black dots correspond to the experimental data. The linear momenta of calculated cold PLF-triggers were filtered with the condition $\theta_{\mathrm{lab}} = 14.5^\circ \pm 1.7^\circ$ and the appropriate energy thresholds to match the experiment.

The charge distribution of primary fragments predicted by the model has a maximum somewhat below the atomic number of projectile and demonstrates a drift towards the lower atomic number of PLF. The agreement of the model calculations with the experimental data for the region in the vicinity of projectile atomic number was obtained. The position of the maximum of the experimental element distribution is well reproduced as well as the shape of it. The discrepancies appear at low Z_{PLF} values, where the net transfer of about 20 nucleons takes place. This is understood because, as it was shown in Sec. 3 the data in this region are composed of variety of reaction mechanisms which are out of scope of the present model (*e.g.*projectile break-up). There is also a reason inherent in the calculation that causes the failure of the model at very massive transfers. The nucleons are transferred in a random walk mode considering each particular nucleon transfer as a process statistically independent on any other preceding or following nucleon transfer. This assumption may be not valid for massive transfer where more correlated processes are expected.

An expected improvement of the description of data is achieved when the deexcitation of hot primary fragments is taken into account. The inclusion of the secondary evaporation has very little effect in the region of Z-values close to that of the projectile and becomes more and more important for decreasing charge number. One may distinguish three regions for

Z-values which are characterised by a different importance of the secondary deexcitation. The first one including the vicinity of the projectile Z-value is only slightly affected by the cooling of primary fragments. On the other hand, the theoretically predicted light fragments with $Z \leq 9$ are produced as secondary fragments and may be interpreted as a result of compound nucleus, target-like, projectile- like fragments evaporation and fragmentation of excited primary projectile-like fragments. For intermediate region of Z_{PLF} the importance of secondary processes steadily increases with decreasing PLF atomic number.

Fig. 3 demonstrates that for Z-values greater than that of the projectile the model with one body dissipation and the wall formula is much more succesfull than the random walk model. Therefore the driving force which directs the net nucleon flux from the heavy target to the light projectile can not be attributed to the phase space factors. On the other hand the succesfull data description of the random walk model with the appended simulation of deexcitation processes is also conclusive. It ilustrates the great importance of the phase space factors in processes where the exit channel mass and charge asymmetry is greater in comparison to the entrance channel.

6. Summary

The comparison of the model predictions with the experimentally obtained charge distribution for $^{40}\mathrm{Ar} + {}^{159}\mathrm{Tb}$ reaction at 9.5 MeV/nucleon (Fig. 3) shows that the random walk model with the phase space factors supplemented by evaporation code reproduces very well the experimental results for fragments with atomic number less than the projectile charge. On the other hand the model of the deep inelastic collisions with one body dissipation is reproducing at least three experimental points for $Z_{\mathrm{PLF}} \geq Z_{\mathrm{proj}}$. Basing on this comparison one could try to make a scenario of heavy ion reaction in the following way. In peripheral collisions the overlap between potentials of the target and the projectile is small and well defined dinuclear system is formed. The idea which takes into account different probabilities for nucleon going to and out of the target and the projectile is positively verified by the comparison with experimental data. These different probabilities are caused by different sizes of the available phase space in heavier and lighter ions. The flow of nucleons is favoured in the direction from the projectile to the target and PLF's much lighter than the projectile are produced. In the course of the collision the overlap of two ions may become so significant that the one nuclear system (monosystem) is formed and the nuclear potential becomes a common one for the whole system. In this situation the idea of two distinct potential centers is not working anymore.

The density of states is the same for both parts of the system and the deep inelasic collisions model, in which the flow of particles in both directions is essentially the same and the predicted drift is towards mass and charge symmetry, is working producing in the exit channel the fragments heavier than the projectile.

REFERENCES

[1] W.U. Schröder, J.R.Huizenga, *Ann. Rev. Nucl. Sci.* **27**, 465 (1977).

[2] H. Machner, D. Protič, G. Riepe, H.G. Bohlen, H. Fuchs, *Phys. Rev.* **C31**, 443 (1985).

[3] S. Wald, S.B. Gazes, C.R. Albiston, Y. Chan, B.G. Harvey, M.J. Murphy, I. Tserruya, R.G. Stoskstad, P.J. Countryman, K. Van Bibber, H. Homeyer, *Phys. Rev.* **C32**, 894 (1985).

[4] F. Rami, J.P. Coffin, G. Guillaume, B. Heusch, P. Wagner, A. Fahli, P. Fintz, *Nucl. Phys.* **A444**, 325 (1985).

[5] R. Bass, *Nuclear Reactions with Heavy Ions*, eds W.Beiglblock, M.Goldhaber, E.H. Lieb, and W. Thirring, Springer–Verlag, Berlin, Heidelberg, New York 1980.

[6] J. Blocki, Y. Bonek, J.R. Nix, J. Randrup, M. Robel, A.J. Sierk, W. Swiatecki, *Ann. Phys.* **113**, 330 (1978).

[7] J. Blocki, H. Feldmeier, W.J. Swiatecki, *Nucl. Phys.* **A459**, 145 (1986).

[8] J. Randrup, *Nucl. Phys.* **A307**, 490 (1979).

[9] B.G. Harvey, *Nucl. Phys.* **A444**, 498 (1985).

[10] J. Cole, *Phys. Rev.* **C35**, 117 (1987).

[11] U. Jahnke, G. Ingold, D. Hilscher, H. Orf, E.A. Koop, G. Feige, R. Brandt, *Lecture Notes in Physics* **178** (1983) 179, ed. W. von Oertzen, Springer-Verlag Berlin, Heidelberg, New York, Tokyo 1983.

[12] E. Kozik, to be published.

[13] J. Blocki, W.J. Swiatecki, Report LBL-12811 (1982).

[14] H.J. Krappe, J.R. Nix, A.J. Sierk, *Phys. Rev.* **C20**, 992 (1979).

[15] Z. Sosin, J. Brzychczyk, K. Grotowski, J.D. Hinnefeld, E.E. Koldenhof, T. Kozik, H.K.W. Leegte, J. Lukasik, S. Micek, R. Planeta, R.H. Siemssen, A. Wieloch, H.W. Wilschut, *Nucl. Phys.* **A574**, 474 (1994).

[16] Z. Sosin, to be published.

[17] J. Wilczynski, K. Siwek-Wilczynska, J. van Driel, S. Gonggrijp, D.C.J.M. Hageman, R.V.F. Janssens, J. Lukasik, R.H. Siemssen, *Phys. Rev. Lett.* **45**, 606 (1980); K. Siwek-Wilczynska, E.H. du Marchie van Voorthuysen, J. van Popta, R.H. Siemssen, J. Wilczynski, *Phys.Rev.Lett.* **42**, 1599 (1979).

[18] R.J. Charity, M.A. McMahan, G.J. Wozniak, R.J. McDonald, L.G. Moretto, D.G. Sarantities, L.G. Sobotka, G. Guarino, A. Pantaleo, L. Fiore, A. Gobbi, K.D. Hildenbrand, *Nucl. Phys.* **A483**, 371 (1988).